

# Transmission of a quantum-dot–silicon-on-insulator hybrid notch filter

Iwan Moreels,<sup>1</sup> Bram De Geyter,<sup>2</sup> Dries Van Thourhout,<sup>2</sup> and Zeger Hens<sup>1,\*</sup>

<sup>1</sup>*Physics and Chemistry of Nanostructures, Ghent University, Krijgslaan 281-S12, BE-9000 Ghent, Belgium*

<sup>2</sup>*Department of Information Technology, Ghent University–IMEC, Sint-Pietersnieuwstraat 41, BE-9000 Ghent, Belgium*

\*Corresponding author: Zeger.Hens@UGent.be

Received December 15, 2008; revised April 2, 2009; accepted April 22, 2009;  
posted April 27, 2009 (Doc. ID 105141); published May 26, 2009

Colloidal PbS and PbSe quantum dots are mixed with polystyrene and spincoated on top of a silicon-on-insulator microring notch filter. We demonstrate that the light propagating through the ring resonator strongly interacts with the quantum-dot doped thin film. This allows us to efficiently tune the output of the notch filter by varying the quantum-dot size and concentration. As a result, the hybrid devices can exhibit critical coupling only for a single resonance or display a constant extinction ratio over a wide spectral range. Considering the promising nonlinear optical properties of colloidal quantum dots, our results open new pathways for all-optical signal processing applications on a silicon platform. © 2009 Optical Society of America

OCIS codes: 130.3120, 160.4236, 310.6845, 350.4238.

## 1. INTRODUCTION

Silicon-on-insulator (SOI) photonics provides a strong platform for all-optical signal processing. It is compatible with complementary metal-oxide semiconductor (CMOS) technology, and devices can be miniaturized down to the micron scale. Consequently, several passive devices have already been demonstrated, ranging from silicon-wire-based structures [1–3] to photonic-crystal-based structures [4,5]. Working on a silicon platform has major drawbacks, however. With a bandgap of 1.12 eV, silicon is not suitable for light detection at telecom wavelengths of 1.3 and 1.55  $\mu\text{m}$ . Furthermore, the indirect bandgap prohibits efficient light emission, and the intrinsic nonlinear optical properties of silicon and the corresponding figure of merit are small [6]. As a result of these restraints, active photonic devices will most probably be of a hybrid nature, where a strongly luminescent and/or nonlinear material with the appropriate bandgap is combined with the advantages of SOI.

Promising candidates for this approach are colloidal semiconductor nanocrystals or quantum dots (Qdots). They are synthesized using wet chemical techniques, offering a wide range of materials and sizes [7–9]. In current state of the art, the particle size dispersion is limited to less than 5%, providing particle suspensions with narrow absorption peaks. As the technique does not rely on a substrate on which to grow the particles, subsequent processing of the nanocrystals can be decoupled from the synthesis. Moreover, since colloidal nanoparticles are suspended in a solvent, a whole set of wet deposition techniques is available, ranging from dip- and spin-coating [10] to Langmuir–Blodgett deposition of monolayers of nanocrystals [11].

In this paper we describe the integration of colloidal lead chalcogenide Qdots (Q-PbS and Q-PbSe) with SOI technology to create a hybrid Qdot–SOI notch filter. We

demonstrate that, by mixing the particles with polystyrene, an optically homogeneous Qdot–polymer composite can be obtained that is suitable for spin-coating on top of the SOI devices. We show that the light propagating through the silicon wires strongly interacts with the Qdots in the doped thin film. The loss of the coated notch filters is calculated from the transmission spectrum and compared to the Qdot absorption coefficient. Efficient tuning of the output characteristics of the Qdot–SOI hybrid notch filter by varying the Qdot size and volume fraction is demonstrated.

## 2. QDOT SYNTHESIS

Q-PbSe is prepared using the synthesis of Murray *et al.* [8]. The synthesis and size-dependent optical properties have recently been reported in [12,13]. Q-PbS is prepared using a modified version of the synthesis of Cademartiri *et al.* [9]. Briefly, a stock solution containing 0.16 g of sulfur dissolved in 15 mL of oleylamine (OLA) is heated to 120 °C for half an hour and afterward cooled down to room temperature. In a three-neck flask, 0.56 g of  $\text{PbCl}_2$  is mixed with 10 mL of OLA and heated to 150 °C. After 30 min, 3 mL of the sulfur stock solution is mixed with 3 mL of OLA and swiftly injected into the three-neck flask. After 20 min, the reaction is quenched by the addition of 20 mL of butanol and 10 mL of methanol. To tune the desired nanocrystal size, the reaction temperature is varied between 75–150 °C, and, if desired, 225  $\mu\text{L}$  of tri-*n*-octylphosphine is added to the injected sulfur solution to increase the available Q-PbS size range. After centrifugation and decantation of the supernatants, the Q-PbS is suspended in toluene.

After synthesis, the OLA capping is substituted by oleic acid (OA) by the addition of 400  $\mu\text{L}$  of OA to the toluene suspension, followed by precipitation of the particles with

methanol. After a second centrifugation and decantation step, the OA capped Q-PbS is resuspended in toluene.

### 3. OPTICAL PROPERTIES

Bulk PbS and PbSe are narrow bandgap materials ( $E_{g,\text{PbS}}=0.41$  eV,  $E_{g,\text{PbSe}}=0.28$  eV). Due to quantum confinement, the bandgap of colloidal Q-PbS and Q-PbSe can be increased to more than 1 eV. This means that by simply varying the particle size, these nanocrystals cover the entire telecom spectral range (Fig. 1). In combination with their high photoluminescence quantum efficiency [14] and nonlinear optical properties [15,16], they are very attractive materials for light-emitting devices and all-optical signal processing on a silicon platform.

Particle sizes and concentrations are determined from the absorbance spectrum using a sizing curve and the molar extinction coefficient at 400 nm. Following the results obtained on Q-PbSe [12], the Q-PbS sizing curve was determined by measuring the particle diameter  $d$  (nm) with transmission electron microscopy and relating it to the particle band gap  $E_0$  (eV), as measured with absorbance spectroscopy on particles suspended in  $\text{C}_2\text{Cl}_4$ . A fit to our data, supplemented with literature values [9], shows that  $E_0$  varies mainly with  $d^{-1}$ , similar to results obtained on Q-PbSe:

$$E_{0,\text{PbS}} = 0.41 + \frac{1}{0.0252d^2 + 0.283d}. \quad (1)$$

For Q-PbSe, the experimental molar extinction coefficient at 400 nm  $\epsilon_{400}$  scales with the particle volume. The data agree well with the theoretical result calculated using the bulk PbSe refractive index  $n$ , extinction coefficient  $k$ , and the solvent refractive index  $n_s$  [12]. This essentially indicates that quantum confinement no longer plays a significant role at energies well above the bandgap. Since PbS has a similar band structure, we assume that the Q-PbS molar extinction coefficient at 400 nm is also bulklike. For particles suspended in  $\text{C}_2\text{Cl}_4$  ( $n_s=1.53$ ), we obtained the following result using  $n=3.96$  and  $k=3.34$  [17]:

$$\epsilon_{400,\text{PbS}} = 0.0233 \cdot d^3 \text{ cm}^{-1}/\mu\text{M}. \quad (2)$$

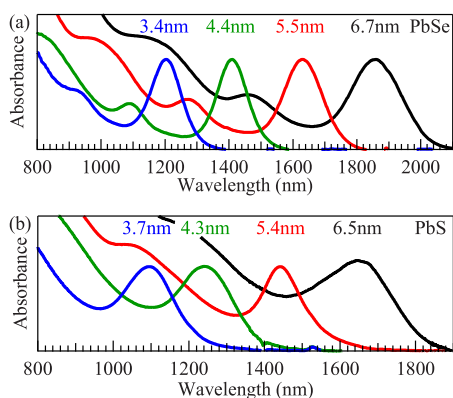


Fig. 1. (Color online) Typical series of absorbance spectra for (a) PbSe and (b) PbS nanocrystals. The absorption peaks shift to shorter wavelengths as the particle size decreases.

### 4. SPIN-COATING

Thin Qdot doped polystyrene films are prepared by suspending a small amount of Qdots in a mixture of polystyrene (PS) and toluene (8 m% of PS in toluene), followed by spin-coating the mixture at 2000 rpm. As neither the polystyrene nor the Qdots evaporate upon spinning, the Qdot volume fraction in the thin film  $f$  (in %) can be calculated from the respective volume fractions of polystyrene  $f_{\text{PS}}$  and of the nanocrystals  $f_{\text{Qdot}}$  in the suspension prior to deposition:

$$f = \frac{f_{\text{Qdot}}}{f_{\text{Qdot}} + f_{\text{PS}}} \cdot 100. \quad (3)$$

Typical absorbance spectra of Q-PbSe doped thin films spin-coated on a glass substrate (Q-PbSe size 5.2 nm,  $f$  varying between 1–5%), are shown in Fig. 2 and compared to the absorbance spectrum of a pure (transparent) PS film and the Q-PbSe suspension. The interference fringes observed in the pure PS thin film demonstrate that it is optically flat. From the spectral position of the interference extrema, a thickness of  $\sim 1 \mu\text{m}$  is estimated, using a PS refractive index of 1.6. For the Qdot doped thin film with  $f=1\%$ , the interference pattern remains clearly visible, albeit now superimposed on the Qdot absorbance. This shows that we have obtained an optically flat and homogeneous Qdot doped thin film. When increasing the Qdot doping to  $f=2\%$ , the interference pattern is less discernible, possibly due to the increased Qdot absorbance or small differences in thin film thickness. More importantly however, at wavelengths beyond the bandgap transition we observe a spectrally flat transmission, indicating that light scattering remains negligible. For the thin film with  $f=5\%$ , this is no longer the case. Although the bandgap transition is still clearly visible, we observe a strong tail extending to long wavelengths. This suggests that at  $f=5\%$  the Qdots start to cluster during deposition, leading to light scattering. In conclusion, good-quality films are obtained up to  $f=2\%$ . At higher volume fractions, the results suggest that Qdot clustering leads to losses induced by both the Qdot absorbance and scattering.

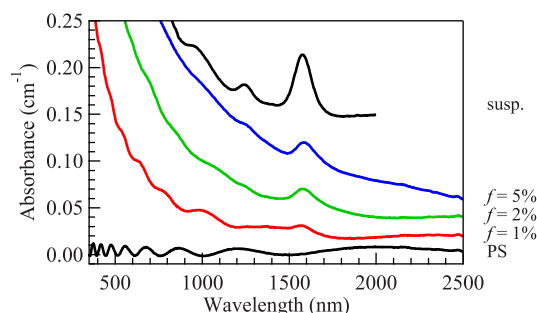


Fig. 2. (Color online) Absorbance spectra for undoped (transparent) PS and Q-PbSe doped PS thin films with varying Q-PbSe volume fraction  $f$  spin-coated on a glass substrate. Interference fringes are observed for pure PS and the Qdot doped thin films with  $f=1\%$  and  $2\%$ . For  $f=5\%$ , a tail extending to long wavelengths indicates that scattering losses are not negligible at this volume fraction. The absorbance spectrum of the Q-PbSe suspended in  $\text{C}_2\text{Cl}_4$  is shown for comparison (top trace). All spectra are offset for clarity.

## 5. INTEGRATION WITH AN SOI NOTCH FILTER

The devices studied here consist of an SOI racetrack ring resonator coupled to a straight photonic wire [Fig. 3(a)]. Typically, the wire has a width of 450 nm and a height of 220 nm. The ring has a length  $L$  of 39.4  $\mu\text{m}$ , with a coupling section of 4  $\mu\text{m}$  and a bend radius of 5  $\mu\text{m}$ . The gap between the ring resonator and the photonic wire equals  $\sim 200$  nm.

Only when the effective length of the ring resonator is equal to an integral number of wavelengths will efficient coupling to the ring resonator mode occur, hereby creating a notch filter. A typical transmission resonance for our SOI notch filter is shown in Fig. 3(b).

The propagating mode in a photonic wire is not fully confined to the silicon core. Simulations of the mode profile using FIMMWAVE, a 2D waveguide mode solver software package, demonstrate that the evanescent tail extends 50–60 nm into the buried oxide underneath and into the PS cladding on top of the wire (Fig. 4). From the mode profile, we calculate a PS filling factor of 0.17, i.e., 17% of the mode power is confined to the PS cladding. Due to absorption in the Qdot doped thin PS film, the light propagating through a photonic wire can therefore experience significant losses after coating.

To reduce these effects, the Qdot doped film is deposited only on the notch filter. Successful local deposition of a monolayer of Qdots using the Langmuir–Blodgett technique has already been demonstrated on predefined areas of flat substrates and SOI devices [11]. A similar approach is used here to deposit a Qdot doped PS film on top of an SOI notch filter. A 1  $\mu\text{m}$  thick photoresist layer is first spin-coated on top of the SOI device. With optical lithography, the resist is selectively removed from the ring resonator, opening an area of 30 by 30  $\mu\text{m}$  around the ring. When spin-coating the Qdot doped polystyrene on top of this stack, direct contact between the SOI access waveguides and the film is hereby avoided, restricting the interaction of the light with the Qdot thin film to the ring resonator.

## 6. TRANSMISSION OF A HYBRID NOTCH FILTER

For the resonance at  $\lambda_0 = 1554.1$  nm, shown in Fig. 3(b), a Q-factor of  $\sim 14000$  and extinction ratio of  $ER = -12.5$  dB is obtained. To gain more insight into the elements determining this Q-factor and extinction ratio, we write the resonance line width  $F$  (full width at half-maximum, equal to  $\lambda_0/Q$ ) and the normalized resonance depth  $D$  (equal to  $10^{ER/10}$ ) in terms of the field amplitude

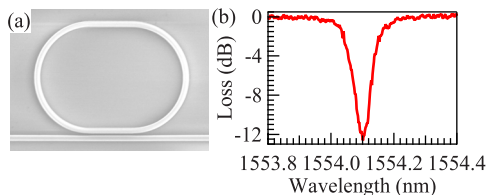


Fig. 3. (Color online) (a) Scanning electron microscope image of a typical SOI notch filter. (b) Transmission spectrum of a notch filter around 1.55  $\mu\text{m}$ .

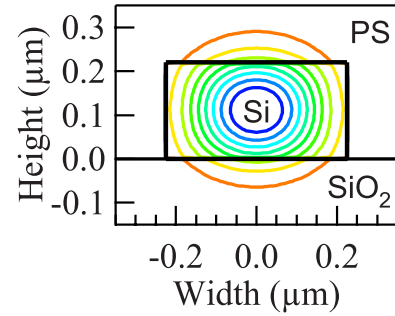


Fig. 4. (Color online) Simulation of the optical mode profile of a wire with a width of 450 nm and a height of 220 nm. The mode expands 50–60 nm into the PS cladding on top and the oxide underneath.

transmission  $a$  per round trip of the light in the ring and the field amplitude transmission  $t$  of the ring–wire coupling section [18]. Here,  $a=1$  implies a lossless ring resonator, and  $t=1$  means that all light is transmitted through the coupling section, i.e., no light is coupled into the ring resonator.

$$F = \frac{(1-at)\lambda_0^2}{\pi L n_g \sqrt{at}}, \quad (4)$$

$$D = \frac{(a-t)^2}{(1-at)^2}. \quad (5)$$

The group index  $n_g$  is obtained from the spectral positions of the ring resonances and the free spectral range  $FSR$ :

$$n_g = \frac{\lambda_0^2}{L \cdot FSR}. \quad (6)$$

For the uncoated ring, we find  $n_g = 4.38$ , which yields  $a \approx t = 0.99$ . Clearly, the low loss and high transmission result in the high Q-factor, while the large extinction ratio is due to critical coupling ( $a=t$ ).

We performed one local deposition of undoped PS on top of an SOI notch filter and six depositions of Qdot doped PS. The thin film properties are summarized in Table 1.

When measuring the transmission spectrum of the PS coated notch filter, we observed a strong decrease in extinction ratio to only  $-2.5$  dB [Fig. 5(a)]. Calculation of  $a$  and  $t$  for the PS coated ring yields  $a \approx 0.99$  and  $t = 0.95$  around 1550 nm. Clearly, the loss is unaffected by the deposition of the PS thin film. The transmission, however, is strongly reduced [note that, due an increased coupling

**Table 1. Summary of the Thin Film Properties for the Six Samples Used**

Sample	Qdot	$\lambda_{\text{res}}$ (nm)	size (nm)	$f$ (%)
1	Q-PbSe	1490	4.8	1.3
2	Q-PbSe	1550	5.1	1.5
3	Q-PbSe	1612	5.4	1.8
4	Q-PbS	1550	5.9	0.75
5	Q-PbS	1550	5.9	2.3
6	Q-PbS	1550	5.9	6.6

<sup>a</sup>  $\lambda_{\text{res}}$  denotes the spectral position of the first absorption peak or bandgap.

<sup>b</sup>  $f$  is the Qdot volume fraction in the spin-coated thin film.

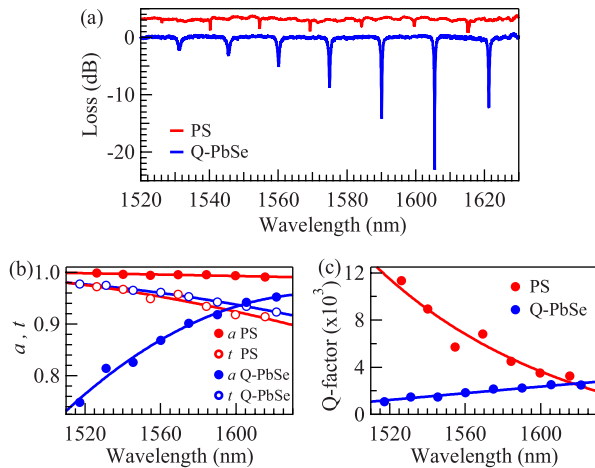


Fig. 5. (Color online) (a) Transmission spectra of a notch filter coated with pure PS and Q-PbSe doped PS. (b) Resulting loss per round trip  $a$  and transmission  $t$ . A strong decrease of  $a$  is observed after doping, while  $t$  is unaffected by the presence of the Q-PbSe. (c) The Q-factor is strongly reduced after incorporation of the nanocrystals due to the decrease in  $a$ .

of the light to the ring resonator at longer wavelengths,  $t$  decreases with increasing wavelength, Fig. 5(b)]. Simulations of the mode profile in a photonic wire as a function of refractive index of the cladding layer  $n_{\text{clad}}$  show that the penetration depth of the evanescent tail increases with increasing  $n_{\text{clad}}$ . The higher penetration depth improves the coupling between the wire and the ring resonator, which explains the reduced transmission after PS deposition.

Figure 5(b) shows  $a$  and  $t$  for the PS coated notch filter over a wavelength range of 1510–1630 nm. The figure also shows that doping the PS layer with a volume fraction  $f=1.3\%$  of Q-PbSe (sample 1) does not significantly change  $t$  but leads to a strong reduction of  $a$ , especially around 1520 nm. By this decrease however, critical coupling is restored at 1605.5 nm [Fig. 5(a)]. The increased losses also reduce the Q-factor of the Q-PbSe coated ring resonator. Around 1550 nm, the Q-factor decreases from  $Q \approx 8000$  for pure PS, to  $Q \approx 1650$  for Q-PbSe doped PS [Fig. 5(c)].

## 7. TUNING OF THE TRANSMISSION SPECTRUM

From  $a$ , the absorption coefficient  $\alpha$  of the ring is calculated as  $\alpha = -20(\log a)/L$  (dB/cm). Figure 6(a) shows the resulting  $\alpha$  for samples 1–3 superimposed on the Q-PbSe absorbance spectra. The excellent correlation between both clearly shows that the loss is due to absorption in the Qdot doped thin film on top of the ring resonator. The results also demonstrate that the absorption at a specific wavelength can easily be tuned by simply varying the Q-PbSe size.

To demonstrate the versatility of our approach, we also prepared notch filters with a Q-PbS doped PS coating. In this case, the increased width of the first absorption peak [Fig. 1(b)] prohibits efficient tuning of the hybrid notch filter transmission by varying the Q-PbS size; however, varying the Q-PbS volume fraction in the PS film also

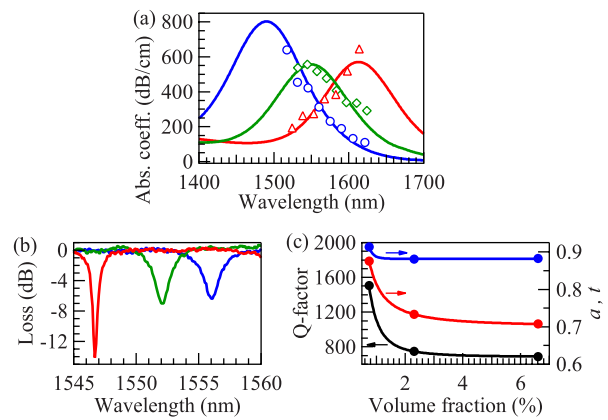


Fig. 6. (Color online) (a) The absorption coefficient  $\alpha$  of samples 1 ( $\circ$ ), 2 ( $\diamond$ ), and 3 ( $\triangle$ ) shows an excellent correlation with the Q-PbSe absorbance spectrum. (b) By increasing the Q-PbS volume fraction in the PS film, the resonance shifts to longer wavelengths. (c) The Q-factor also decreases. This is due to a decrease in  $a$ , as  $t$  remains fairly constant.

leads to strong changes in the transmission spectrum. This is demonstrated in Fig. 6(b) (samples 4–6). First, the resonances shift to longer wavelengths with increasing  $f$ . Under conditions of low doping levels, the effective index of the Qdot doped PS film scales linearly with  $f$ . Due to the high refractive index of PbS ( $n_{\text{PbS}}=4.5$ ) and the high sensitivity of SOI rings to the refractive index of the cladding, even low Qdot volume fractions lead to an efficient tuning of the resonance wavelength. In addition, the extinction ratio and Q-factor decrease [Fig. 6(c)]. Calculation of  $a$  and  $t$  shows that this is due to a strong decrease in  $a$ , as  $t$  remains fairly constant. This again demonstrates that  $a$  is determined by the Qdot absorption. Note that, similar to the Q-PbSe doped thin film with  $f=5\%$  shown in Fig. 2, sample 6 ( $f=6.6\%$ ) possibly suffers from light scattering, implying that the value for  $a$  is no longer solely due to the Qdot absorbance. However, this does not influence the general conclusion that the transmission

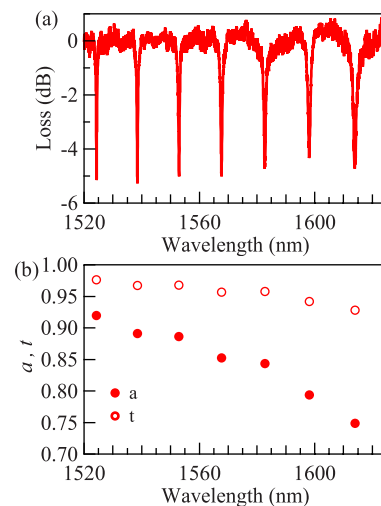


Fig. 7. (Color online) Transmission spectrum of a notch filter coated with a Q-PbSe doped PS film (sample 3). A constant extinction ratio of  $-4.84$  dB is observed over a 120 nm wavelength range.

properties of the Q-PbS hybrid notch filter can be efficiently tuned by varying the Qdot volume fraction.

Figure 5(a) already demonstrated that for sample 1, where  $a$  increases with increasing wavelength critical coupling is achieved at 1605.5 nm, while the shape of the Q-PbSe absorbance spectrum ensures that the extinction ratio strongly decreases for other wavelengths. For Q-PbSe with an absorption peak at 1612 nm, exactly the opposite can be achieved. Figure 7(a) shows that in this case, a nearly constant extinction ratio of  $-4.84$  dB with a standard deviation of 0.27 dB is measured over a wavelength range of 1510–1630 nm, again demonstrating that the transmission spectrum can be tuned to a high degree by choosing the appropriate Qdot size and volume fraction. Figure 7(b) confirms that  $a$  and  $t$  indeed both decrease with increasing wavelength, leading to a nearly constant  $D$  over the entire spectral range [Eq. (5)].

## 8. CONCLUSIONS

We have shown that Q-PbSe and Q-PbS can be mixed with polystyrene to produce optically flat and homogeneous quantum dot doped thin films for volume fractions of up to 2%. Thin films were spin-coated on top of an SOI notch filter, and transmission spectra of these coated devices were used to calculate the transmission per round trip  $a$  and transmission of the coupling section  $t$ . The loss of the coated rings is due to absorption in the quantum-dot doped thin film. Consequently, as was demonstrated with notch filters coated with Q-PbSe doped PS, varying the Qdot size leads to a strong modification of the transmission spectrum. For particles with an absorption peak at 1490 nm, a high extinction ratio of  $-23.7$  dB is achieved only for a single resonance, while when using particles with a peak at 1612 nm a nearly constant extinction ratio of  $-4.84$  dB can be achieved over a 1510–1630 nm wavelength range. In addition, as is demonstrated using Q-PbS doped PS, the resonance wavelengths of the notch filter can be efficiently tuned by varying the quantum dot concentration in the film.

Controlling both the size and concentration of the Qdots in the thin films therefore leads to a high degree of control over the transmission characteristics of these quantum dot–SOI hybrid devices. Considering the high photoluminescence efficiency [14], the high nonlinear refractive index [15], and observation of absorption saturation [16] in these colloidal nanocrystals, the devices presented here provide a promising route toward all-optical signal processing on a silicon platform.

## ACKNOWLEDGMENTS

I.M. acknowledges the Institute for the Promotion of Innovation through Science and Technology in Flanders (IWT-Vlaanderen) for a scholarship. The Belgian Science Office (IAP-P6/10) and the EU Network of Excellence ePIXnet are also acknowledged for financial support.

## REFERENCES

1. W. Bogaerts, P. Dumon, D. Van Thourhout, D. Taillaert, P. Jaenen, J. Wouters, S. Beckx, V. Wiaux, and R. G. Baets, "Compact wavelength-selective functions in silicon-on-insulator photonic wires," *IEEE J. Sel. Top. Quantum Electron.* **12**, 1394–1401 (2006).
2. Y. A. Vlasov and S. J. McNab, "Losses in single-mode silicon-on-insulator strip waveguides and bends," *Opt. Express* **12**, 1622–1631 (2004).
3. T. Tsuchizawa, K. Yamada, H. Fukuda, T. Watanabe, J. Takahashi, M. Takahashi, T. Shoji, E. Tamechika, S. Itabashi, and H. Morita, "Microphotonic devices based on silicon microfabrication technology," *IEEE J. Sel. Top. Quantum Electron.* **11**, 232–240 (2005).
4. Y. Akahane, T. Asano, B. S. Song, and S. Noda, "High-Q photonic nanocavity in a two-dimensional photonic crystal," *Nature (London)* **425**, 944–947 (2003).
5. E. Kuramochi, H. Taniyama, T. Tanabe, A. Shinya, and M. Notomi, "Ultra-high-Q two-dimensional photonic crystal slab nanocavities in very thin barriers," *Appl. Phys. Lett.* **93**, 111112 (2008).
6. M. Dinu, F. Quochi, and H. Garcia, "Third-order nonlinearities in silicon at telecom wavelengths," *Appl. Phys. Lett.* **82**, 2954–2956 (2003).
7. C. B. Murray, D. J. Norris, and M. G. Bawendi, "Synthesis and characterization of nearly monodisperse CdE ( $E = \text{S, Se, Te}$ ) semiconductor nanocrystallites," *J. Am. Chem. Soc.* **115**, 8706–8715 (1993).
8. C. B. Murray, S. H. Sun, W. Gaschler, H. Doyle, T. A. Betley, and C. R. Kagan, "Colloidal synthesis of nanocrystals and nanocrystal superlattices," *IBM J. Res. Dev.* **45**, 47–56 (2001).
9. L. Cademartiri, E. Montanari, G. Calestani, A. Migliori, A. Guagliardi, and G. A. Ozin, "Size-dependent extinction coefficients of PbS quantum dots," *J. Am. Chem. Soc.* **128**, 10337–10346 (2006).
10. J. M. Luther, M. Law, Q. Song, C. L. Perkins, M. C. Beard, and A. J. Nozik, "Structural, optical and electrical properties of self-assembled films of PbSe nanocrystals treated with 1,2-ethanedithiol," *ACS Nano* **2**, 271–280 (2008).
11. K. Lambert, I. Moreels, D. Van Thourhout, and Z. Hens, "Quantum dot micropatterning on Si," *Langmuir* **24**, 5961–5966 (2008).
12. I. Moreels, K. Lambert, D. De Muynck, F. Vanhaecke, D. Poelman, J. C. Martins, G. Allan, and Z. Hens, "Composition and size-dependent extinction coefficient of colloidal PbSe quantum dots," *Chem. Mater.* **19**, 6101–6106 (2007).
13. I. Moreels and Z. Hens, "On the interpretation of colloidal quantum-dot absorption spectra," *Small* **4**, 1866–1868 (2008).
14. A. L. Rogach, A. Eychemuller, S. G. Hickey, and S. V. Kershaw, "Infrared-emitting colloidal nanocrystals: synthesis, assembly, spectroscopy, and applications," *Small* **3**, 536–557 (2007).
15. I. Moreels, Z. Hens, P. Kockaert, J. Loicq, and D. Van Thourhout, "Spectroscopy of the nonlinear refractive index of colloidal PbSe nanocrystals," *Appl. Phys. Lett.* **89**, 193106 (2006).
16. M. Brumer, M. Sirota, A. Kigel, A. Sashchiuk, E. Galun, Z. Burshtein, and E. Lifshitz, "Nanocrystals of PbSe core, PbSe/PbS, and PbSe/PbSe<sub>x</sub>S<sub>1-x</sub>, core/shell as saturable absorbers in passively Q-switched near-infrared lasers," *Appl. Opt.* **45**, 7488–7497 (2006).
17. H. Kanazawa and S. Adachi, "Optical properties of PbS," *J. Appl. Phys.* **83**, 5997–6001 (1998).
18. A. Yariv, "Universal relations for coupling of optical power between microresonators and dielectric waveguides," *Electron. Lett.* **36**, 321–322 (2000).